Determination of Protein Secondary Structure and Solvent Accessibility Using Site-Directed Fluorescence Labeling. Studies of T4 Lysozyme Using the Fluorescent Probe Monobromobimane†

Steven E. Mansoor,‡ Hassane S. Mchaourab,§ and David L. Farrens*,‡

Departments of Biochemistry and Molecular Biology, Oregon Health Sciences University, 3181 Southwest Sam Jackson Park Drive, Portland, Oregon 97201-3098, and National Biomedical ESR Center, Biophysics Research Institute, Medical College of Wisconsin, 8701 Watertown Plank Road, Milwaukee, Wisconsin 53226

Received June 10, 1999; Revised Manuscript Received October 7, 1999

ABSTRACT: We report an investigation of how much protein structural information could be obtained using a site-directed fluorescence labeling (SDFL) strategy. In our experiments, we used 21 consecutive single-cysteine substitution mutants in T4 lysozyme (residues T115−K135), located in a helix−turn−helix motif. The mutants were labeled with the fluorescent probe monobromobimane and subjected to an array of fluorescence measurements. Thermal stability measurements show that introduction of the label is substantially perturbing only when it is located at buried residue sites. At buried sites (solvent surface accessibility of <40 Å^2), the destabilizations are between 3 and 5.5 kcal/mol, whereas at more exposed sites, $\Delta\Delta G$ values of ≤ 1.5 kcal/mol are obtained. Of all the fluorescence parameters that were explored (excitation λ_{max}, emission λ_{max}, fluorescence lifetime, quantum yield, and steady-state anisotropy), the emission λ_{max} and the steady-state anisotropy values most accurately reflect the solvent surface accessibility at each site as calculated from the crystal structure of cysteine-less T4 lysozyme. The parameters we identify allow the classification of each site as buried, partially buried, or exposed. We find that the variations in these parameters as a function of residue number reflect the sequence-specific secondary structure, the determination of which is a key step for modeling a protein of unknown structure.

Fluorescence spectroscopy is ideal for studying the structure, function, local environment, and dynamics of proteins (*1*−*5*). Unfortunately, frequently no fluorescent molecule (or site to which to attach one) is present in the region of interest. Site-directed mutagenesis has recently solved this problem, by allowing the introduction of a probe anywhere in the structure that the folded protein will tolerate, enabling a more systematic application of fluorescence to structural studies. Recently, a number of studies have shown the power this new ability gives to fluorescence studies of protein structure and dynamics (*6*−*8*, *9*).

Similarly, it has recently been established that through the combination of site-directed mutagenesis and electron paramagnetic resonance (EPR) spectroscopy, regular segments of protein secondary structure can be identified [for a review, see Hubbell et al. (*10*)]. In these types of studies (called site-directed spin-labeling, or SDSL), cysteine residues are systematically engineered, one after another, into a defined region of a protein. A nitroxide spin-label is then attached to the cysteines, and the mobility and solvent accessibility of each label are determined from analysis of the EPR data. Through the combination of SDSL scanning and distance measurements between pairs of nitroxides, movement between regions of a protein can be detected (*11*, *12*) and three-dimensional protein models can be generated (*13*−*15*). Key to the SDSL approach is the fact that introduction of the spin-label probe does not result in large changes in the structure at the level of the backbone fold.

The purpose of this paper is to examine systematically what level of protein structural information can be obtained using an analogous site-directed fluorescence labeling (SDFL) approach. Thus, we set out to determine (1) what affects the introduction of the fluorescent probe has on a protein structure and (2) which fluorescent parameters reliably encode protein structural information. For this purpose, we determined the structural and functional consequences of introducing the fluorescent probe monobromobimane (mBBr)[1] into a protein sequence. An example is shown in Scheme 1. We chose mBBr as it is a relatively small, uncharged fluorescent label (about the size of a tryptophan or spin-label), is sensitive to changes in the polarity of the surrounding solvent, and has been well characterized by Kosower and colleagues (*16*). Furthermore, London and co-workers have recently shown that bimane is an excellent probe for use in SDFL studies of membrane proteins (*17*). As a model protein system, we chose T4 lysozyme, because of the vast amount of thermodynamic and structural data that is available for this protein. The studied region consists of a

† This work was supported by Grants EY12095-01 to D.L.F. and EY12018 to H.S.M. from the National Eye Institute.

* To whom correspondence should be addressed. Telephone: (503) 494-0583. Fax: (503) 494-8393. E-mail: farrensd@ohsu.edu.

‡ Oregon Health Sciences University.

§ Medical College of Wisconsin.

[1] Abbreviations: mBBr, monobromobimane; MOPS, 3-(*N*-morpholino)propanesulfonic acid; EDTA, *N*,*N*′-1,2-ethanediylbis[*N*-(carboxymethyl)glycine] disodium salt; Tris, 2-amino-2-(hydroxymethyl)-1,3-propanediol; T4L, T4 lysozyme; IPTG, isopropyl β-thiogalactoside.

10.1021/bi991331v CCC: $18.00
Published on Web 11/17/1999

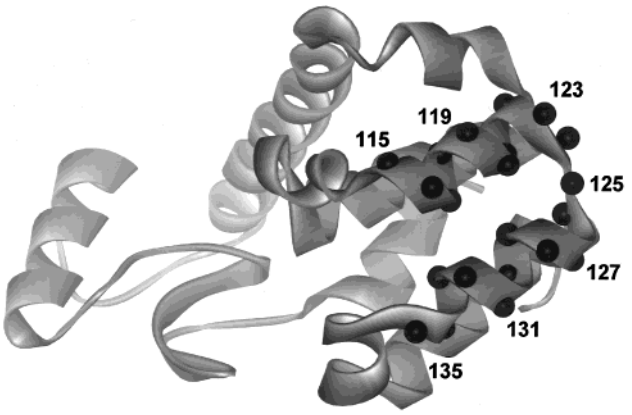

FIGURE 1: Model of cysteine-less WT T4 lysozyme based on the crystal structure showing the location of cysteine mutant sites that were labeled with monobromobimane. The black balls show the relative positions of each α-carbon substituted with a cysteine residue.

Scheme 1: Reaction of the Monobromobimane (mBBr) Label with a Cysteine Residue To Produce an S-Bimane Side Chain

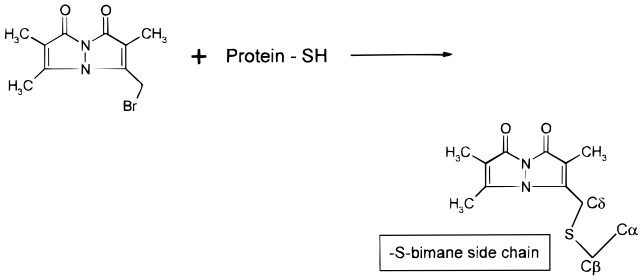

helix−turn−helix motif, and thus provided enough structural variation to allow generalized conclusions to be made (Figure 1).

The experiments involved constructing 21 sequential cysteine mutants in T4 lysozyme (T4L), reacting each with the fluorescent mBBr label, and then subjecting the lot to analysis using an array of fluorescence techniques. The general conclusions from our work are (i) the mBBr label is only substantially perturbing to the protein stability and function when introduced into a buried site, (ii) the solvent accessibility of the protein is reliably reflected in the fluorescence emission λ_{max} and steady-state anisotropy values, and (iii) the fluorescence excitation λ_{max}, fluorescence lifetime, and quantum yield values do not simply reflect the three-dimensional structure of the protein. Several strengths of the SDFL approach we describe include the small amount of sample required for the measurements, the commercial availability and relative ease of use of the methods described, and the ability of the bimane label to monitor the apparent polarity at sites on a protein structure.

MATERIALS AND METHODS

Materials. Monobromobimane (mBBr) was purchased from Molecular Probes. Quinine sulfate monohydrate was purchased from Aldrich Chemical Co. The reagents L-cysteine and *Escherichia coli* strain B were from Sigma. The solvent dioxane was purchased from Mallinckrodt. Neutral density filters, long-pass filters, and interference filters were from Oriel Corp. All cuvettes were from Uvonics. All buffer components were purchased from Fisher-Biotech except guanidine hydrochloride, which was purchased from Gibco BRL. The cysteine-free pseudo-wild-type lysozyme gene containing the substitutions C54T and C97A (*18*) was kindly provided by F. W. Dahlquist (University of Oregon, Eugene, OR). This will be called the "wild type" or T4L.

The buffers used were as follows: buffer A, 50 mM MOPS, 50 mM Tris, and 1 mM EDTA (pH 7.6); buffer B, 0.1 M Tris-HCl and 0.1 M Na_2EDTA; buffer C, 20 mM Tris-HCl and 1 mM $CaCl_2$ (pH 8.0); buffer D, 20 mM Tris, 20 mM MOPS, 0.02% sodium azide, 1 mM EDTA, and 1 mM DTT (pH 7.6); buffer E, 20 mM KH_2PO_4 and 25 mM KCl (pH 3.0); and buffer F, 50 mM MOPS, 50 mM Tris, 1 mM EDTA (pH 7.6), and 3 M guanidine hydrochloride.

Construction of T4L Mutants. Site-directed mutagenesis was carried out using polymerase chain reaction (PCR) methods (*19*). Two new restriction sites, *Sph*I and *Xba*I, were introduced into the previously described plasmid using the overlap extension method. Synthetic oligonucleotides containing the X to cysteine substitution and overlapping either of the restriction sites were used to generate PCR fragments. The PCR fragments were then digested and ligated into the appropriate cloning vector. All mutant constructs were confirmed by DNA sequencing. Mutants are named by specifying the original residue, the number of the residue, and the new residue, in that order. For example, the code T115C indicates that the native threonine residue at amino acid position 115 was mutated to a cysteine.

Expression and Purification of T4L Mutants. Mutant proteins were expressed as described previously (*20*). Briefly, competent K38 *E. coli* cells were transformed with the T4L cysteine mutant plasmid (*21*), and protein production was induced in log phase cultures (OD_{595} of 1.2) by the addition of IPTG (1 mM). After being shaken for 120 min at room temperature, the cells were harvested by centrifugation (3500 rpm for 15 min). The cell pellet was resuspended in 30 mL of buffer D; the cells were lysed using a French press, and the suspension was then spun at 10 000 rpm for 30 min and filtered (0.45 μm). DTT was added to the filtered cell solution to a final concentration of 20 mM, and after 30 min, the solution was loaded onto a Pharmacia Biotech HiTrap 1 mL SP anion exchange column equilibrated with buffer A. The samples were eluted with a salt gradient (ramped from 0 to 1 M over the course of 20 min). The protein concentration was determined by UV absorption at 280 nm using an extinction coefficient for T4 lysozyme of 23 327 L cm^{-1} mol^{-1}. Protein purification was assessed by SDS−PAGE, and all mutants were judged to be at least 90% pure.

Fluorescence Labeling of T4L Mutants. Labeling of each lysozyme mutant was accomplished using a 10× molar excess of the fluorescent label in buffer F at 4 °C overnight. The labeled protein was separated from free label using a Pharmacia Biotech HiTrap 5 mL desalting column (equilibrated with buffer A). The labeling efficiency for each mutant was calculated from the absorption spectrum measured using a Shimadzu UV 1601 UV−vis dual-beam spectrophotometer, using the following extinction coefficients: ϵ_{280} = 23 327 L cm^{-1} mol^{-1} for T4 lysozyme and ϵ_{380} = 5000 L cm^{-1} mol^{-1} for mBBr (an ϵ_{280} of 17 727 L cm^{-1} mol^{-1} was used for mutant W126C). The contribution from mBBr at 280 nm was subtracted before calculating the protein concentrations. Incubation of the cysteine-less WT protein showed that

the level of background labeling was less than 1% as judged by fluorescence.

The nomenclature used throughout the rest of the paper is outlined below. Mutants labeled with mBBr are named by specifying the original residue, the number of the residue, and the suffix B_1, indicating the monobromobimane label. For example, the code $T115B_1$ indicates that the native threonine residue at amino acid position 115 has been mutated to a cysteine and reacted with the mBBr label.

Protein Activity Assays. The enzymatic activity of each mBBr-labeled mutant was assessed by monitoring changes in light scattering as the T4L digests a suspension of peptidoglycan (*22*). In brief, peptidoglycan was isolated (*23*) and suspended in buffer C for the activity assays. Each assay measured light intensity at 365 nm (5 nm band-pass) from a 358 nm (1 nm band-pass) excitation beam using a PTI steady-state fluorescence spectrophotometer (PTI). To initiate the assays, 5 μL of mBBr-labeled lysozyme mutant (2 μM in buffer A) was added to 350 μL of peptidogycan solution, and the samples were stirred continuously during the measurement. The activity rates were determined from the initial slope of a plot of change in light intensity versus time. The mutant's activities are reported as a percentage of the wild type's activity. Measurements were taken in triplicate at 20 °C and averaged.

Assessment of Thermodynamic Stability. The stability of each mBBr-labeled mutant was assessed by analyzing its thermal unfolding properties (*24*, *25*), by monitoring the tryptophan fluorescence emission intensity at 320 and 350 nm as a function of temperature. At the point of thermal denaturation, the emission at each of these wavelengths changes due to the solvent sensitive property of tryptophan fluorescence (*24*, *26*).

The thermal melts used 2 μM labeled protein dialyzed against buffer E and were carried out using the PTI steady-state fluorescence spectrophotometer in a T-format. The samples were excited at 280 nm, and the tryptophan fluorescence emission was monitored at 350 and 320 nm, using 3 nm slit widths on both the excitation and emission monochromators. The melts involved ramping the temperature from 6 to 80 °C at a rate of 2 °C/min, after which the samples were cooled to 6 °C to determine the extent of protein refolding. The mutants exhibited greater than 75% refolding, as judged by the extent to which the ratio returned to its starting value. The melts were carried out in duplicate, and the reported T_m values are the average of the two melts. To avoid photooxidation, the samples were only exposed to the UV excitation light for 5 s/min during the temperature ramping process.

The thermal melt data were analyzed assuming a two-state model (native folded state and totally denatured state) in equilibrium (*24*, *25*):

$$\text{folded (F)} \leftrightarrow \text{unfolded (U)}$$

At equilibrium, the above assumption can be used to obtain

$$\Delta G = \Delta H_u - T_m \Delta S_u = 0$$

where ΔG refers to the free energy for the unfolding reaction, ΔH_u is the enthalpy of unfolding, ΔS_u is the entropy of unfolding, and T_m is the melting temperature (the temperature at which half of the protein is in the native, folded state and half is in the denatured, unfolded state).

Rearranging the above equation (at equilibrium) results in

$$T_m = \frac{\Delta H_u}{\Delta S_u}$$

Using this relationship, the T_m of each mBBr-labeled mutant was determined by fitting the steady-state fluorescence melt data (F) to the following equation (*24*) to obtain values for ΔH_u and ΔS_u:

$$F = \frac{F_{0N} + s_N T + (F_{0U} + s_U T) \times e^{(-\Delta H_{u^\circ} + T\Delta S_{u^\circ})/RT}}{1 + e^{(-\Delta H_{u^\circ} + T\Delta S_{u^\circ})/RT}}$$

where F_{0N} is the fluorescence intensity of the native state and F_{0U} is the fluorescence intensity of the unfolded state. The variables s_N and s_U represent the temperature dependence (baseline slope, assumed to be linear) of the fluorescence for the native state and unfolded state, respectively, $\Delta H_u°$ is the enthalpy change, and $\Delta S_u°$ is the entropy change for the two-state unfolding reaction.

With the assumptions put forth by Becktel and Schellman (*27*), $\Delta\Delta G$ values for each mBBr-labeled T4 lysozyme mutant were calculated using the approximation

$$\Delta\Delta G = \Delta T_m \times \Delta S_{wt}$$

where ΔT_m is the difference in melting temperatures between the mutant and the wild type and the ΔS_{wt} value is the change in entropy between the folded and denatured states of the wild-type protein. The thermodynamic properties of each mutant were determined by measuring the ΔT_m and then calculating the $\Delta\Delta G$ value [using the approximation that $\Delta\Delta G = \Delta T_m \times \Delta S_{wt}$ (*27*)], relative to the cysteine-less WT protein. All calculations and nonlinear least-squares analyses were carried out using Sigma Plot 5.0 (SPSS Inc.).

Solvent Sensitivity of Model Bimane Compound (mBBr-Cys). The sensitivity of the mBBr absorbance spectra to solvent polarity was assessed by reacting mBBr (40 μM) with L-cysteine (200 μM), and then measuring the absorbance spectrum in dioxane/water mixtures ranging from 0 to 100% (v/v) dioxane at 22 °C. Similarly, the solvent sensitivity of the mBBr-Cys fluorescence properties was determined using a 2 μM solution of the mBBr-Cys from the stock described above and the same conditions. Wavelength maxima were determined from the first derivative of the spectra.

Steady-State Fluorescence Measurements of Mutants. The steady-state fluorescence measurements of mBBr-labeled mutants were taken at 22 °C, using a 2 μM sample in buffer A and the PTI fluorometer, unless noted otherwise. The fluorescence excitation spectra were measured from 300 to 450 nm, using an integration time of 1 s, a step size of 1.0 nm, and a corrected emission signal at 490 nm. Excitation slits were 1 nm band-pass, and emission slits were set at 15 nm band-pass. The fluorescence emission spectra were measured from 395 to 600 nm while exciting at 381 nm, using an integration time of 1 s, a step size of 1.0 nm, and a corrected emission signal. To maximize the resolution in the emission data, emission slits were kept at 1.0 nm band-

pass and excitation slits were set at 10 nm band-pass. All measurements used real-time excitation correction.

Quantum Yield Measurements. The quantum yields for each mBBr-labeled mutant were measured using the relation (*28*)

$$\Phi_x = \Phi_{st} * \frac{F_x}{F_{st}} \frac{OD_{st}}{OD_x}$$

where subscripts st and x refer to standard and unknown solutions, respectively, Φ is the quantum yield, F is the relative integrated fluorescence intensity, and OD is the optical density at the exciting wavelength. Quinine sulfate (quantum yield equal to 0.55 in 1 N H_2SO_4) was chosen as the standard. Corrected emission spectra were taken using 360 nm excitation (3 nm slit width), from 370 to 700 nm (1 nm band-pass) at 22 °C for 10 μM samples of the bimane-labeled lysozyme mutants and for the quinine sulfate standard. The buffer intensity was subtracted from each sample and from the standard before integration from 370 to 625 nm.

Fluorescence Lifetime Measurements. The fluorescence lifetimes of the mBBr mutants were measured using a PTI Laserstrobe fluorescence lifetime instrument, which consists of a nitrogen-pumped dye laser and a stroboscopic detector. Measurements were taken at 22 °C, using 381 nm excitation pulses (fwhm $\sim$ 1.5 ns), while monitoring the emission through a long pass filter (>470 nm). Measurements used 250 μL of a 10 μM sample placed in a 4 mm black-jacketed cuvette and represent two averages of five shots per point, collected in 150 channels. A 298−435 nm band-pass filter was also used on the excitation beam. The instrument response function (IRF) was determined by measuring light scatter from a solution of Ludox through a 400 nm broadband interference filter. Data were acquired using an arithmetic data collection method, and analyzed using the commercial PTI software. Both a two-exponential decay model and the Exponential Series Method (ESM) (*29*−*32*) were used in the analysis. The ESM method fits the decay data using a series of exponentials as a probe function with fixed, logarithmically spaced lifetimes and variable pre-exponentials to differentiate between continuous lifetime distributions and discrete, multiexponential decays. The ESM analysis was allowed to fit the decay data using 100 discrete lifetimes of varying amplitude from 0.1 to 30 ns and proceeded until χ^2 was minimized.

Steady-State Fluorescence Anisotropy Measurements. The steady-state fluorescence anisotropy (r) was measured using the PTI instrument, by comparing the polarization of the light emitted to the polarization of the excitation light:

$$r = \frac{I_{||} - GI_{\perp}}{I_{||} + 2GI_{\perp}}$$

where $I_{||}$ and $I_{\perp}$ refer to the intensity of fluorescence emission parallel and perpendicular to the plane of excitation light, respectively. The G-factor was determined before measuring the anisotropy of each mutant to correct for bias in the monochromator. Anisotropy measurements were carried out at 15 °C using each lysozyme mutant (2 μM) in buffer A. Excitation was at 381 nm (4 nm slits), and emission was collected at 475 nm (5 nm slits). The measurements were done in triplicate, and the average steady-state anisotropy was reported.

Calculation of the Solvent-Accessible Surface Area. The solvent-accessible surface area of each residue in the range of T115−K135 was calculated using a probe radius of 1.4 Å, using the program ICM Lite (*33*, *34*), and the crystal structure coordinates of a cysteine-less WT T4 lysozyme mutant (PDB file 1L63; *35*).

Time-Resolved Fluorescence Emission Spectra. Time-resolved emission spectra were measured using the PTI Laserstrobe instrument. Briefly, this involved measuring the emission intensity at a user defined time after the excitation laser pulse. To generate an emission scan, the measuring process was repeated at different wavelengths, a process automated by the PTI instrument. The time for the scan after the excitation pulse was selected using a Stanford Digital delay line. Spectra were recorded using the monochromator (5 nm band-pass) 1 ns after the excitation pulse, and then again after a time corresponding to three average lifetime decays. A 361 nm excitation wavelength was used to reduce light scattering over the emission wavelength region that was measured, although similar results were obtained using 381 nm excitation.

Fourier Transform Spectral Density Calculation. Fourier transform power spectra, $P(\omega)$, were calculated for the average of the emission λ_{max} values and the steady-state anisotropy values and compared to the power spectrum of the residue solvent accessibility (accessibility calculated from the crystal structure of T4 lysozyme). The calculations were performed following methods previously described (*14*, *36*, *37*). Briefly, the fast Fourier transform of the data was determined and the spectral density calculated by summing the square of the real and the square of the imaginary portions of the fast Fourier transform. The calculations were made using Sigma Plot 5.0 (Jandel Scientific).

RESULTS

Our goal in this paper was to assess quantitatively whether site-directed fluorescence labeling (SDFL) could be used to obtain protein structural information at the level of the backbone fold. We also wanted to determine if the solvent-sensitive properties of bimane could be used to estimate apparent polarity at the site of labeling. Toward these goals, we prepared 21 single-cysteine substitution mutants (Figure 1) and reacted each with the fluorescent probe mBBr (Scheme 1). The region we chose to study (amino acids T115−K135) represents an α-helix−turn−helix secondary motif (*35*, *38*), and thus serves as a good case on which to test our methodology. The labeled mutants were first characterized and then subjected to an array of fluorescence measurements, the results of which are described below.

Characterization of mBBr-Labeled T4L Mutants. Table 1 reports the labeling efficiency as well as the functional and thermodynamic stability of the mBBr-labeled mutants. As can be seen, all the T4L mutants could be labeled at an essentially 1:1 ratio, whereas the cysteine-less "WT" protein exhibited a less than 1% level of labeling (data not shown). The functional activity results, which measured the labeled mutants' ability to breakdown a preparation of *E. coli* cell walls (*22*), indicate that some mutants have impaired activity, especially those at buried sites. The thermodynamic stability

Table 1: Characterization of Bimane-Labeled T4 Lysozyme Mutants

mutant	mol of label per mol of protein	activity (% of WT)	ΔT_m[a] at 320 nm (°C)	ΔT_m[b] at 350 nm/320 nm (°C)	$\Delta\Delta G$[c] (kcal/mol) at 320 nm	$\Delta\Delta G$[d] (kcal/mol) at 350 nm/320 nm
T115C	1.0	2	−1.0	−0.5	−0.3	−0.1
N116C	1.0	25	−2.1	−2.0	−0.6	−0.6
S117C	1.0	0	−10.1	−11.4	−3.1	−3.2
L118C	1.0	3	−14.7	−14.2	−4.5	−4.0
R119C	0.9	69	−0.8	−0.5	−0.2	−0.1
M120C	0.8	80	−5.5	−5.3	−1.7	−1.5
L121C	1.0	0	−15.1	−15.4	−4.6	−4.4
Q122C	1.3	51	−1.2	−1.0	−0.4	−0.3
Q123C	1.0	71	−0.1	0.3	0.0	0.1
K124C	0.9	61	−2.7	−2.5	−0.8	−0.7
R125C	1.0	72	−1.9	−1.6	−0.6	−0.5
W126C	0.9	5	−12.1	−11.6	−3.7	−3.3
D127C	0.9	40	−1.4	−1.4	−0.4	−0.4
E128C	1.1	41	−1.3	−1.8	−0.4	−0.5
A129C	1.1	0	−11.5	−12.4	−3.5	−3.5
A130C	0.9	76	−3.1	−4.7	−1.0	−1.3
V131C	0.9	122	0.8	0.7	0.2	0.2
N132C	0.8	80	1.5	1.8	0.5	0.5
L133C	1.1	18	−22.0	−19.5	−6.8	−5.5
A134C	0.9	138	−0.9	−1.0	−0.3	−0.3
K135C	0.8	15	−0.8	−0.6	−0.2	−0.2

[a] Wild-type T_m (determined from 320 nm fluorescence) = 52.9 °C. [b] Wild-type T_m (determined from 350 nm/320 nm fluorescence) = 52.4 °C. [c] $\Delta\Delta G = \Delta T_m \times \Delta S_{wt}$ (ΔS_{wt} = 305.7 cal mol^{-1} K^{-1}), calculated using the 320 nm data. [d] $\Delta\Delta G = \Delta T_m \times \Delta S_{wt}$ (ΔS_{wt} = 284.6 cal mol^{-1} K^{-1}), calculated using the 350 nm/320 nm data.

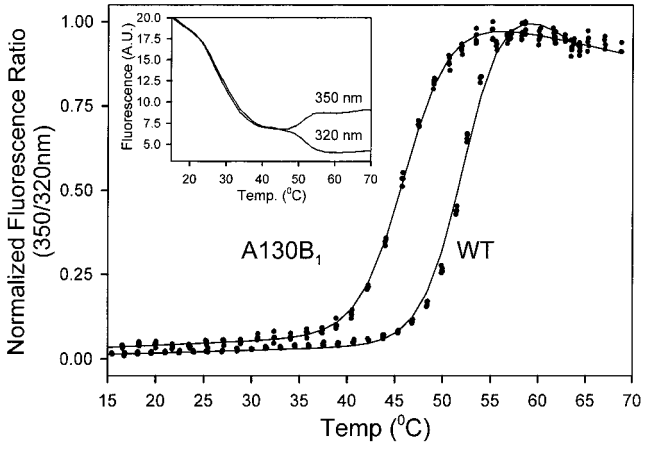

FIGURE 2: Thermal denaturation of WT T4 lysozyme and a representative mutant. The plot shows the relative fluorescence change in T4L determined from the ratio of 350 nm to 320 nm fluorescence as the temperature is increased. The inset shows the raw data from the melting experiments. Note that at both wavelengths a temperature-dependent decrease in intensity is observed, followed by a relative increase in 350 nm emission as the protein unfolds.

was measured by monitoring the intrinsic tryptophan fluorescence with increasing temperature (*24*). Table 1 reports the thermal unfolding temperatures determined by monitoring the fluorescence signal at a single wavelength, 320 nm, and by monitoring the ratio of fluorescence at 350 nm to the fluorescence at 320 nm. The inset of Figure 2 shows how the fluorescence signal changes at 350 and 320 nm with increasing temperature. Notice the fluorescence changes that occur at the unfolding transition (due to the exposure of the tryptophan residues upon unfolding). Examples of thermal melt curves obtained using the ratio of fluorescence (350 nm:320 nm) is shown if Figure 2. These measurements were used to calculate the $\Delta\Delta G$ values reported in Table 1. Both approaches produce almost identical results, although the theoretical basis for using the single-wavelength values is more firmly established (*24*). Note that the ratio of fluorescence at 350 nm to that at 320 nm eliminates the sloping baseline that is caused by the inherent temperature dependence of tryptophan fluorescence. The measurements indicate that protein stability is generally impaired only for mutants whose labeled site is buried in the protein structure.

Spectral Properties of mBBr-Labeled Mutants. Figure 3 shows how the spectral properties of mBBr-labeled mutants can vary at different sites. The spectra show that an exposed site ($E128B_1$) has a much greater red shift to its spectral properties than a buried site ($L133B_1$). Table 2 reports the λ_{max} values of all the mutants. Previous studies have shown that mBBr is a solvent-sensitive fluorophore (*39*); thus, the differences in the spectral shifts of the mBBr-labeled mutants are likely related to this sensitivity. This subject will be explored further in the Discussion.

We tested whether the solvent-sensitive properties of mBBr could be used to establish a scale for evaluating the "structural classification" of a given mutant. To provide a reference calibration, we measured the spectral properties of mBBr reacted with cysteine in different mixtures of dioxane and water. The measurements of this model compound (hereafter termed mBBr-Cys) enabled us to compare the mBBr mutant values with an "apparent polarity" scale. While the apparent polarity values thus generated are based on an arbitrarily chosen reference, they allow for an instrument-independent comparison scale; i.e., any systematic error in wavelength accuracy for a particular instrument is normalized by measuring the model compound apparent polarity scale on the same instrument.

In all the spectroscopic measurements, the λ_{max} of mBBr-Cys varies as a function of the solvent dielectric constant (achieved by varying the dioxane concentration). As shown in the insets of Figure 3, two linear regions are observed in these measurements, one from $\epsilon = 2$ to ~10, and a second

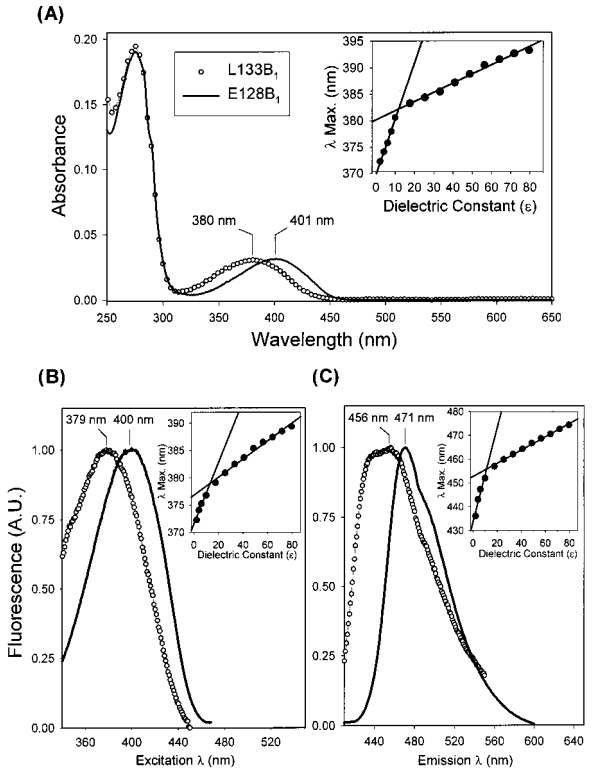

FIGURE 3: Solvent sensitivity of the absorbance, fluorescence excitation, and fluorescence emission of mBBr. Examples show mBBr on an exposed site on T4L ($E128B_1$, black line) and at a buried site ($L133B_1$, ○). The inset in each figure shows the linear dependence of mBBr-Cys on the solvent polarity, achieved by varying the dielectric constant of the solvent through the use of different combinations of water and dioxane. (A) Solvent sensitivity of absorbance spectra. (B) Solvent sensitivity of fluorescence excitation spectra. (C) Solvent sensitivity of fluorescence emission spectra.

from $\epsilon \sim 18$ to 80. Each of these linear regions could be fit to a line of the form $W = mD + b$, where W is the absorbance wavelength (nanometers), m is the slope of the line, D is the dielectric constant (ϵ), and b is the y-intercept. The results of the spectral calibration measurements are summarized as follows: absorbance, $W = 1.06(\text{nm}/\epsilon)D + 369.8$ nm (for $\epsilon = 2-10$), and $W = 0.18(\text{nm}/\epsilon)D + 380.2$ nm (for $\epsilon \sim 18-80$); fluorescence excitation, $W = 0.56(\text{nm}/\epsilon)D + 371.5$ nm (for $\epsilon = 2-10$), and $W = 0.17(\text{nm}/\epsilon)D + 376.8$ nm (for $\epsilon \sim 18-80$); and fluorescence emission, $W = 1.98(\text{nm}/\epsilon)D + 433.7$ nm (for $\epsilon = 2-10$), and $W = 0.28(\text{nm}/\epsilon)D + 452.7$ nm (for $\epsilon \sim 18-80$). The apparent polarity values thus generated by these relationships are used in the Discussion. Note that the two different linear regions of mBBr sensitivity to solvent polarity have previously been observed by Kosower and colleagues (*39*).

Measurement of the mBBr Fluorophore Mobility. The second parameter expected to reflect the local atomic density around the site of attachment is the mobility of the probe. The mobility of each mBBr label attached to the T4L mutants was assessed by steady-state fluorescence anisotropy measurements. Variations are observed in the anisotropy values (Table 2). Generally, labels at buried sites exhibit a higher steady-state anisotropy than those at exposed sites, indicating that the dense packing at buried sites restricts the rotational mobility of the probe. Similar to the shift in the emission wavelength, the anisotropy values at contact sites are distinct from those of buried and exposed sites. Thus, three distinct classes of sites can be identified on the basis of the steady-state anisotropy. The error bars shown in Table 2 are the standard error uncertainty in the mean of the three anisotropy measurements for each mutant.

Table 2: Spectral Characterization of Bimane-Labeled T4 Lysozyme Mutants

mutant	absorbance λ_{max} (nm)	excitation[a] λ_{max} (nm)	emission[b] λ_{max} (nm)	quantum yield (Φ)	mBBr bimane[c] SS anisotropy ($\times 10^{-3}$)
$T115B_1$	387.9	385.7	468.6	0.15	102.0 ± 6.2
$N116B_1$	388.2	386.3	469.6	0.18	107.9 ± 0.2
$S117B_1$	385.5	383.6	462.9	0.20	155.4 ± 3.7
$L118B_1$	387.1	384.5	467.7	0.16	143.0 ± 1.3
$R119B_1$	387.4	386.2	471.1	0.15	92.7 ± 3.0
$M120B_1$	380.9	380.2	467.5	0.26	105.0 ± 1.8
$L121B_1$	386.1	385.7	464.7	0.08	128.8 ± 6.3
$Q122B_1$	388.6	386.8	467.2	0.24	113.4 ± 4.8
$Q123B_1$	389.1	387.4	469.8	0.24	88.9 ± 5.0
$K124B_1$	393.3	388.8	471.2	0.04	146.0 ± 8.0
$R125B_1$	383.2	381.7	472.7	0.23	83.3 ± 6.0
$W126B_1$	387.7	385.4	467.3	0.23	126.1 ± 0.7
$D127B_1$	388.1	387.5	470.5	0.20	68.5 ± 1.7
$E128B_1$	400.5	399.6	470.9	0.19	135.3 ± 0.9
$A129B_1$	386.9	388.3	466.8	0.09	116.4 ± 3.7
$A130B_1$	383.4	383.3	467.6	0.26	128.8 ± 0.6
$V131B_1$	381.3	378.1	468.4	0.22	101.3 ± 1.6
$N132B_1$	387.8	386.2	468.8	0.35	96.4 ± 0.6
$L133B_1$	379.8	378.9	456.3	0.08	174.8 ± 9.6
$A134B_1$	379.8	377.8	462.0	0.17	161.9 ± 3.1
$K135B_1$	391.5	389.7	472.4	0.17	60.3 ± 4.1

[a] Emission collected at 490 nm. [b] Excitation at 381 nm. [c] The uncertainty is in the mean of three measurements.

Quantum Yield. The relative fluorescence decay properties of each labeled mutant were checked by measuring its quantum yield (*28*). The values reported in Table 2 are averages of two measurements. It can be seen that the quantum yields of the mBBr-labeled mutants vary in a sequence-specific fashion, with values ranging from 0.35 down to 0.04.

Fluorescence Lifetimes. The fluorescence lifetimes of the mBBr-labeled T4L mutants were measured and analyzed using both a two-exponential fit and the exponential series method (*29*−*31*). The two-exponential fit results are reported in Table 3. The fits from the exponential series method are graphically shown in Figure 4. Although the fluorescence lifetime of mBBr-Cys in water is well-described using just a single-exponential decay, the lifetimes of mBBr attached to T4L differ dramatically, depending upon the location of the label on the mutant (Table 3 and Figure 4). These differences were further explored using the ESM analysis, which show for several mutants, the fluorescence decays are well fit only using a broad distribution of lifetimes and/or multiple distributions of lifetimes. This is especially clear in mutants $L121B_1$, $K124B_1$, $W126B_1$, $A129B_1$, and $L133B_1$ (Figure 4). This broad distribution and multiple populations of lifetimes could be due to several factors, including the conformational heterogeneity of the flourescent label in either the ground state or excited states, or the heterogeneity of the protein structure.

Time-Resolved Fluorescence Emission Spectra. As a followup to the fluorescence lifetime studies, the environment around the mBBr labels in the excited state was probed for several mutants by recording time-resolved emission spectra. These experiments measured the emission spectrum 1 ns after the excitation pulse, and then again after three average

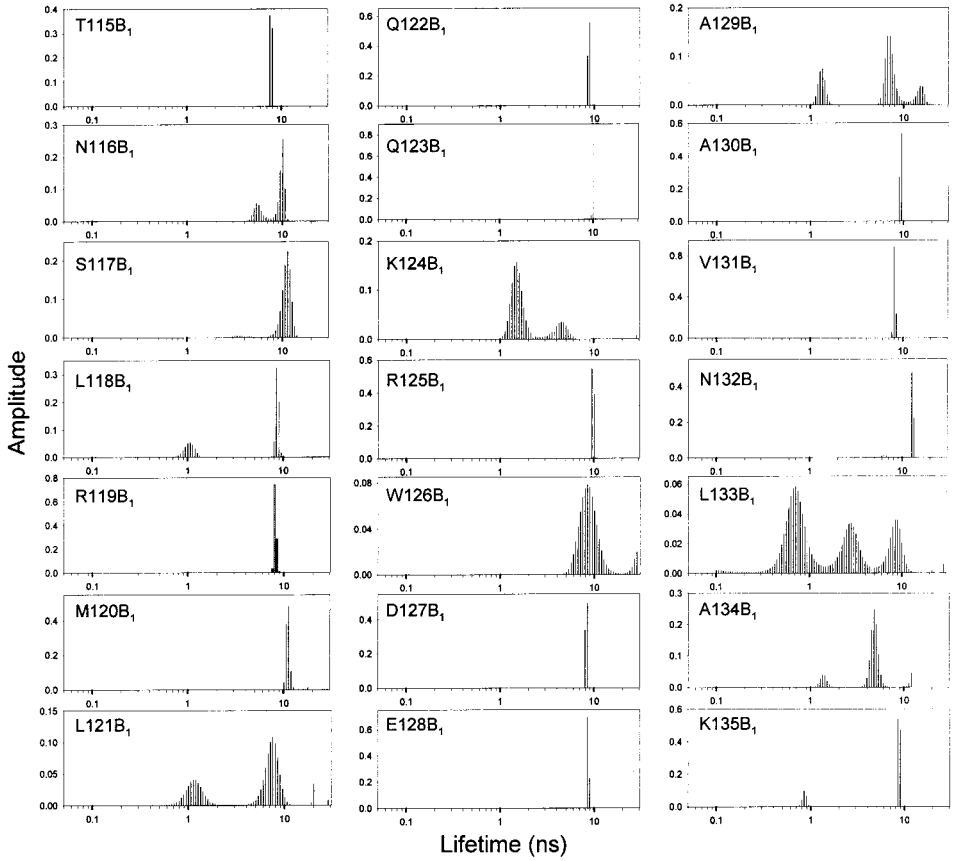

FIGURE 4: Fluorescence decay data from the 21 mBBr-labeled T4L mutants analyzed using the exponential series method. Data were fit by allowing the amplitude (*y*-axis) of 100 evenly spaced lifetimes (*x*-axis) to vary until the best fit of the data was achieved (defined as $\chi^2 = 1$). Notice that a broad distribution of lifetimes is required to fit the data for many of the buried sites (e.g., $L121B_1$, $W126B_1$, $A129B_1$, and $L133B_1$), suggesting heterogeneity of the emitting species.

Table 3: Results of the Two-Exponential Lifetime Fits for the Fluorescence Decay Measurements[a]

mutant	τ_1 (ns)	α_1	f_1 (%)	τ_2 (ns)	α_2	f_2 (%)	χ^2
$T115B_1$	7.86	0.86	93	1.13	0.07	7	1.10
$N116B_1$	8.83	0.84	86	1.59	0.14	14	0.81
$S117B_1$	11.12	0.83	89	1.02	0.10	11	1.14
$L118B_1$	9.63	0.67	66	1.63	0.35	34	1.28
$R119B_1$	8.28	0.92	98	0.08	0.02	2	0.98
$M120B_1$	11.22	0.94	95	0.18	0.05	5	1.07
$L121B_1$	8.52	0.68	63	1.55	0.40	37	1.05
$Q122B_1$	8.82	0.96	70	0.24	0.42	30	1.21
$Q123B_1$	9.78	0.75	99	0.002	0.01	1	1.05
$K124B_1$	4.86	0.29	17	1.20	1.41	83	1.04
$R125B_1$	9.67	1.06	91	0.01	0.10	9	1.04
$W126B_1$	9.12	0.73	80	0.53	0.18	20	1.01
$D127B_1$	8.38	1.04	92	0.75	0.09	8	0.96
$E128B_1$	8.70	1.06	100	0.86	0.01	−	0.85
$A129B_1$	8.75	0.91	61	0.95	0.57	39	0.88
$A130B_1$	9.64	0.84	90	1.04	0.09	10	0.94
$V131B_1$	8.19	1.03	90	0.50	0.12	10	1.26
$N132B_1$	11.80	0.92	86	0.29	0.15	14	1.04
$L133B_1$	7.01	0.47	32	1.00	1.00	68	0.98
$A134B_1$	5.10	1.07	66	0.58	0.56	34	0.95
$K135B_1$	8.76	0.79	79	1.12	0.21	21	0.92

[a] Excitation wavelength of 381 nm; emission collected using a >470 nm long-pass filter. τ_1 and τ_2 are lifetimes in nanoseconds. α_1 and α_2 are pre-exponential factors for τ_1 and τ_2, respectively. f_1 and f_2 are the fractional amplitudes of each lifetime. $f_1 = 100 \times \alpha_1/\Sigma\alpha_i$, and $f_2 = 100 \times \alpha_2/\Sigma\alpha_i$. χ^2 is the chi-squared value of the fit.

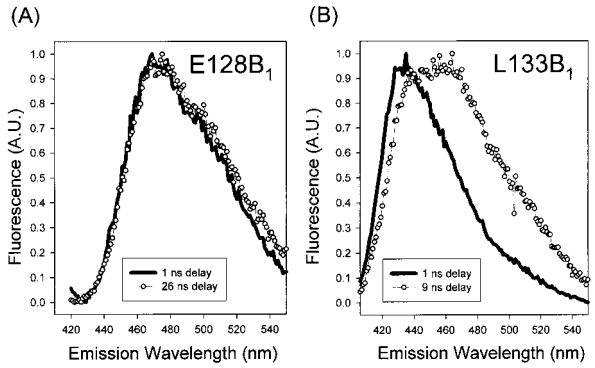

FIGURE 5: Time-resolved emission spectra of $E128B_1$ (exposed site) and $L133B_1$ (buried site). (A) Normalized time-resolved emission spectra of solvent-exposed mutant $E128B_1$. Spectra were recorded 1 ns after the pulse (black line) and again after 26 ns (○). The latter delay time was chosen to allow three average lifetimes to pass, after which ~85% of the excited molecules will have decayed. Note that no change in emission λ_{max} is observed. (B) Normalized time-resolved emission spectra of buried mutant $L133B_1$, taken 1 ns after the pulse (black line) and again after 9 ns (○). Again, the latter time was chosen to allow three average lifetimes to pass. Notice the large, approximately 20 nm red shift that occurs in the emission λ_{max}, indicating that a time-dependent solvent rearrangement around the excited bimane species has occurred.

lifetime decays had occurred (after which approximately 85% of the initial excited species has decayed). Two representative examples are given in Figure 5, showing mutants $E128B_1$ (solvent-exposed) and $L133B_1$ (buried). Note that in mutant $E128B_1$, the emission λ_{max} is ~470 nm immediately (1 ns) after the excitation pulse and remains so when measured after three average lifetime decays have passed (26 ns). In contrast, emission from mBBr attached at a buried site (L133C) starts

at ~435 nm 1 ns after the excitation pulse, but can be seen to shift to ~460 nm after three lifetime decays (9 ns). These results indicate that the excited-state behavior of mBBr depends on whether it is in a buried or exposed location on the protein.

DISCUSSION

Background. As stated in the introductory section, our goal in this paper was to test how much protein structural information could be obtained using a site-directed fluorescence labeling (SDFL) strategy. Thus, we systematically introduced the fluorescent label mBBr into 21 different sites on T4 lysozyme, and then subjected the samples to a battery of measurements (fluorescence excitation, emission, lifetime, quantum yield, and steady-state anisotropy). These results were then compared with the known structure of T4L. Below, we discuss (i) the effect of the mBBr label on the T4L protein function and stability, (ii) how the SDFL results compare with the structure of T4L, and (iii) speculation about why some spectral parameters provide more structural information in an SDFL study.

(i) Effects of the mBBr Label on T4L Protein Function and Stability. Except mutant T115C (Table 1), enzymatic activity is not abolished when the mBBr label is attached on the surface of the protein. However, buried sites are affected, as was previously observed in studies of spin-labeled T4L mutants (*40*). The thermal stability of the proteins is also worse for buried mutants. It appears that introduction of the mBBr label into sites with less than 40 Å^2 accessible surface area results in a destabilization between 3 and 5.5 kcal/mol. In contrast, for more solvent-exposed sites, the destabilization is less than 1.5 kcal/mol. Matthews' group has established that introduction of volume into a stericly crowded region of T4L destabilizes the protein (*41*); thus, we surmise that the destabilization caused by mBBr at buried sites is due to rearrangements of the core required to satisfy the increased volume of the labeled side chain. Despite these destabilizations, the labeled mutants still exhibit reversible and cooperative thermal unfolding and have melting curves that are very similar to those of the wild-type protein. Analogous results were also seen in spin-label studies of T4L (*40*).

Figure 6 compares the destabilization, represented as $\Delta\Delta G$ values, caused by the introduction of the mBBr label (Table 1) along with the solvent accessibility of the original residue (calculated from the crystal structure of T4L). Notice that destabilization mirrors the solvent accessiblity of the original residue. Most of the sites (15 out of 21) exhibit destabilization of ≤1.5 kcal/mol. Only the extremely buried sites exhibit larger destabilizations (between 3.0 and 5.5 kcal/mol). While the latter destabilization values are not trivial, they are not larger than those resulting from substitution with native amino acids at the same sites (*41*).

(ii) Comparison of Results with the Structure of T4L. Of all the parameters we studied, the fluorescence emission and steady-state anisotropy values of the mBBr-labeled mutants best reflect the T4L protein structure, specifically, the solvent-accessible surface area of residues 115−135 in T4L (Figure 7). Figure 7A shows the calculated solvent accessibility at each residue compared to the measured apparent polarity at each residue plotted versus the residue number.

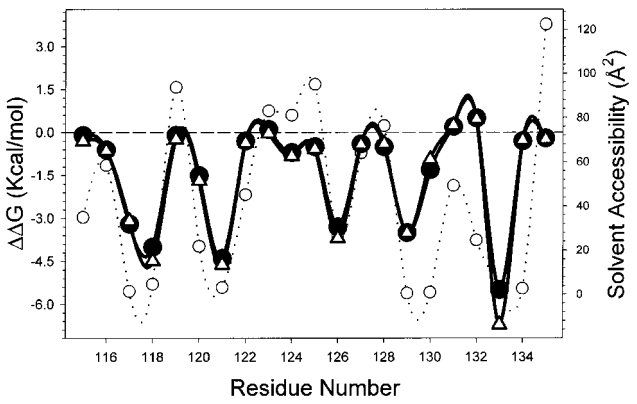

FIGURE 6: Thermodynamic stability of mBBr-labeled mutants. The results compare the residue solvent accessibility (○) with the $\Delta\Delta G$ values from the 350 nm/320 nm thermal melt analysis (●) and the $\Delta\Delta G$ values from the 320 nm analysis (△). The residue solvent accessibility and $\Delta\Delta G$ values at each site were calculated as described in Materials and Methods. The dotted and solid black lines represent a cubic-spline fit of the respective data.

Note that the apparent polarity values were calculated by comparing the emission λ_{max} of the mBBr-labeled mutants with the results from the model mBBr-Cys measurements in dioxane (see Materials and Methods and Results). We hasten to point out there is no single, generally applicable polarity parameter (*2*). However, we chose to reference our results against the apparent polarity scale we derived from mBBr-Cys in dioxane/water because (i) it provides an easily reproducible way to compare values from mBBr-labeled proteins between different laboratories and (ii) it provides a rough feel for solvent polarity on a scale more familiar to biochemists.

Figure 7B compares the fluorescence anisotropy as a function of residue position with the solvent accessibility at each site. A good correlation is evident, although not quite as close as with the emission λ_{max} values. Interestingly, two mutants ($K124B_1$ and $E128B_1$) are anomalous; although these sites are exposed on the crystal structure of T4L, their anisotropy values are unexpectedly high. These two sites are at the location of turns in the protein. Thus, it is possible the attached labels may experience a restriction in mobility not reflected in the accessibility of a relatively smaller molecule (water). Studies are currently under way to resolve these anomalies.

The fluorescence lifetimes also vary with the solvent accessibility, especially in the relative amount of long and short fluorescence lifetime components from the two-exponential fits (Table 3). However, the correlation is not as good as observed for the emission λ_{max} and anisotropy data. This is not surprising, as many processes can affect the decay properties of a fluorescent molecule on a protein, including quenching by the peptide backbone and neighboring amino acids (*2*, *42*, *43*). The latter explanation is supported by the observed variations in quantum yields (Table 2).

The differences in the lifetime data between buried and exposed sites are more pronounced when the decays are analyzed using the exponential series method (ESM). ESM fits the decay data using a number of discrete exponential lifetimes, while allowing the contribution of each lifetime component to vary (*30*). ESM analysis is useful for detecting

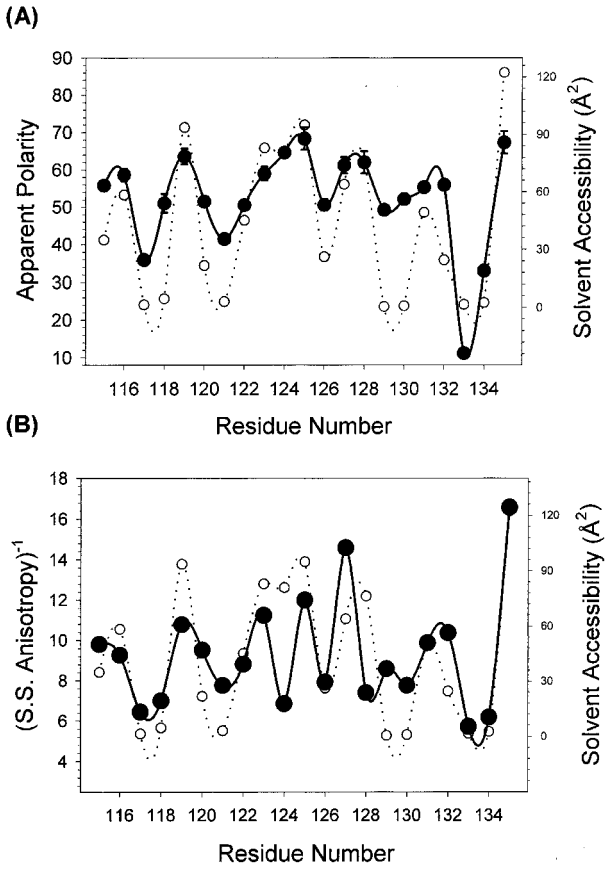

FIGURE 7: Comparison of the calculated residue solvent accessibility with the apparent polarity and the mobility of mBBr at each cysteine substitution site. Note that the mBBr mutants' emission apparent polarity values are derived from the model mBBr-Cys emission measurements in various dioxane/water mixtures, as described in Materials and Methods. (A) Fluorescence emission apparent polarity values at each site (●) compared with the residue solvent accessibility (○). (B) The inverted steady-state fluorescence anisotropy values (●) compared with the residue solvent accessibility (○). Measurements were carried out in triplicate, and the standard errors in the mean values are shown by the error bars. The solid black and dotted lines represent a cubic-spline fit of the respective data. Note that the inverses of the steady-state values are represented to allow direct comparison with the solvent accessibility.

cases where a fluorescent molecule is found in several heterogeneous states, such as in the interior of a protein or membrane. Notice that at the buried sites, a broad distribution of lifetimes is observed, consistent with a heterogeneous population of emitting species. In extremely buried sites, multiple broad distributions are found (see for example Figure 4, mutant L133B$_1$), suggesting that the fluorophore may exist in multiple conformers.

Interestingly, the apparent polarity values obtained from ground-state measurements (absorbance λ_{max} and fluorescence excitation λ_{max}) do not correlate very well with the solvent accessibility (compare Figure 7 with Figure 8). Large discrepancies are seen for M120B$_1$, R125B$_1$, E128B$_1$, and V131B$_1$, which may be caused by perturbation (hydrogen bonding or electrostatic interaction) of the mBBr label in the ground state. Particularly striking is the abnormally high (compared to that of water) apparent polarity of E128B$_1$, which may occur because of the proximity of R125. We are exploring these aspects further, as they may prove to be useful in mapping local polarity or electrostatics on a protein.

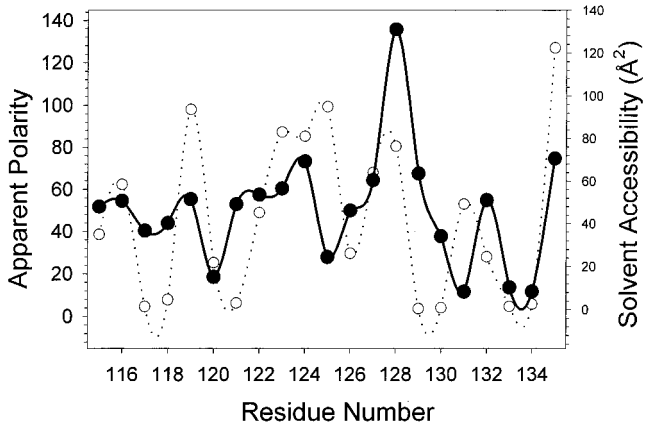

FIGURE 8: Apparent polarities calculated from the fluorescence excitation spectra of mBBr-labeled T4L mutants (●) compared with the original residue solvent accessibility at attachment sites (○). Note that the mBBr mutants' excitation apparent polarity values are derived from the model mBBr-Cys excitation measurements in various dioxane/water mixtures, as described in Materials and Methods. Measurements were carried out in triplicate, and the standard errors in the mean values are shown by the error bars. The solid black and dotted lines represent a cubic-spline fit of the respective data. The apparent polarity values from the fluorescence excitation measurements do not agree with the solvent accessibility at several sites.

(iii) Speculation about Why Some Spectral Parameters Provide More Structural Information in an SDFL Study. The explanation for why the emission anisotropy follows the solvent-accessible surface of the protein is straightforward; depolarization mainly depends on the local mobility of each attached mBBr label. At buried sites, there are more steric restrictions on the label's mobility; thus, the overall anisotropy values are higher. Although the steady-state anisotropy values are affected both by the protein tumbling in solution and by local movements of the attached label, within the set of mutants the data are comparable because the protein tumbling rates are likely the same for all of the mutants. Thus, the depolarization mainly depends on the local mobility of each attached mBBr label. One cautionary note is that a shorter fluorescence lifetime at a buried site will also contribute to a higher steady-state anisotropy value.

Our explanation for why the fluorescence emission λ_{max} and lifetime values are in good agreement with the solvent-accessible protein surface area is more involved, but still straightforward. Bimane in the excited state (mBBr*) undergoes a charge separation that requires the surrounding solvent to rearrange to form more favorable interactions with the new mBBr* species (*39*). Favorable solvent repacking occurs around the mBBr*, lowering its energy and thus resulting in a red shift in its fluorescence emission spectrum. The mBBr labels at exposed sites of the protein can easily undergo solvent repacking. In contrast, the local environment is less able to accommodate the excited mBBr* species at a buried site, and thus the emission occurs out of a higher-energy (and thus blue-shifted) species.

The time-resolved emission spectra of the mutants shown in Figure 5 support the latter hypothesis. These spectra show that the excited-state mBBr* behaves differently at a buried site than at a solvent-exposed site. Any spectral shifts at the E128B$_1$* site are complete within 1 ns after excitation (Figure 5A). In contrast, the spectral shifts observed for the buried

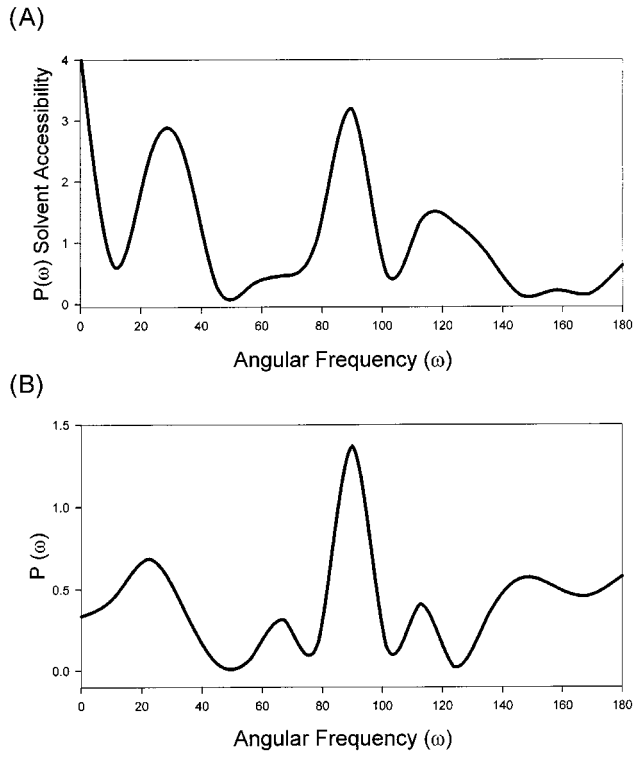

FIGURE 9: Fourier transform spectral density calculations carried out on the fluorescence emission and steady-state data compared with calculations carried out on the solvent accessibility data. (A) Spectral density transforms of the solvent accessibility data. (B) Spectral density transforms of the normalized fluorescence emission apparent polarity values averaged with the normalized steady-state anisotropy values.

E133B_1* (Figure 5B) occur slowly, presumably because of hindered solvent repacking.

Conclusions and Future Directions. We have demonstrated in this paper that an SDFL strategy can be used to estimate the solvent-accessible surface area of a protein and determine its structure at the level of the backbone fold. From our analysis, the fluorescence emission and steady-state anisotropy measurements are easiest to interpret and most faithfully reflect the secondary structure of the protein fold, although information is also certainly encoded in the other spectral parameters. Clearly, the methods outlined here could help in modeling proteins of unknown structure. Recently, Perozo and colleagues have demonstrated the usefulness of analyzing site-directed spin labeling results using Fourier transform spectral density calculations (*14*). In Figure 9, we have extended this approach by comparing the Fourier transform spectral density calculation of the residue solvent accessibility (from the crystal structure) with the spectral density calculation of the combined λ_{max} emission apparent polarity values and steady-state anisotropy values. Similar periodicity components are present in both sets of data. Especially noteworthy is the major peak centered at approximately 90°, which reflects the presence of an α-helix. These types of calculations allow an objective way of quantifying the periodicity of the SDFL data, and would allow one to objectively model an unknown protein structure based on an SDFL study. For example, one could constantly change a protein structure model until the Fourier transform spectral density power spectrum of its solvent accessibility agrees with the SDFL data. In future work, we hope to turn our attention to using such methods to study proteins of unknown structure.

ACKNOWLEDGMENT

We thank Dr. A. Siemiarczuk, Dr. D. Brennan, and Dr. A. Glasfeld for many helpful discussions, and especially Dr. H. P. Bachinger for helpful discussions regarding the thermal melt experiments.

REFERENCES

1. Stryer, L. (1968) *Science 162*, 526−533.
2. Lakowicz, J. R. (1999) *Principles of Fluorescence Spectroscopy*, 2nd ed., Plenum Press, New York.
3. Eftink, M. R. (1991) in *Protein Structural Determination: Methods of Biochemical Analysis* (Suelter, C. H., Ed.) Vol. 35, pp 127−205, John Wiley & Sons, New York.
4. Weber, G. (1997) *Methods Enzymol. 278*, 1−15.
5. Beechem, J. M. (1997) *Methods Enzymol. 278*, 24−49.
6. Barry, J. K., and Matthews, K. S. (1997) *Biochemistry 36*, 15632−15642.
7. Shepard, L. A., Heuck, A. P., Hamman, B. D., Rossjohn, J., Parker, M. W., Ryan, K. R., Johnson, A. E., and Tweten, R. K. (1998) *Biochemistry 37*, 14563−14574.
8. Jung, K., Jung, H., Wu, J., Prive, G. G., and Kaback, H. R. (1993) *Biochemistry 32*, 12273−12278.
9. Gasymov, O. K., Abduragimov, A. R., Yusifov, T. N., and Glasgow, B. J. (1997) *Biochem. Biophys. Res. Commun. 239*, 191−196.
10. Hubbell, W. L., Mchaourab, H. S., Altenbach, C., and Lietzow, M. A. (1996) *Structure 4*, 779−783.
11. Farrens, D. L., Altenbach, C., Yang, K., Hubbel, W. L., and Khorana, H. G. (1996) *Science 274*, 768−770.
12. Yang, K., Farrens, D. L., Hubbell, W. L., and Khorana, H. G. (1996) *Biochemistry 35*, 12464−12469.
13. Poirier, M. A., Xiao, W., Macosko, J. C., Chan, C., Shin, Y.-K., and Bennett, M. K. (1998) *Nat. Struct. Biol. 5*, 765−769.
14. Perozo, E., Cortes, D. M., and Cuello, L. G. (1998) *Nat. Struct. Biol. 5*, 459−469.
15. Koteiche, H. A., Berengian, A. R., and Mchaourab, H. S. (1998) *Biochemistry 37*, 12681−12688.
16. Kosower, E. M., and Kosower, N. S. (1995) *Methods Enzymol. 251*, 133.
17. Wang, Y., Malenbaum, S. E., Kachel, K., Zhan, H., Collier, R. J., and London, E. (1997) *J. Biol. Chem. 272*, 25091−25098.
18. Matsumara, M., and Matthews, B. W. (1989) *Science 243*, 792−794.
19. Ho, S. N., Hunt, H. D., Horton, R. M., Pullen, J. K., and Pease, L. R. (1989) *Gene 77*, 51−59.
20. Sauer, U. H., Dao-pin, S., and Matthews, B. W. (1992) *J. Biol. Chem. 267*, 2393−2399.
21. Inoue, H., Nojima, H., and Okayama, H. (1996) *Gene 96*, 23−28.
22. Tsugita, A., Inouye, M., Terzaghi, E., and Streisinger, G. (1968) *J. Biol. Chem. 243*, 391−397.
23. Becktel, W. J., and Baase, W. A. (1985) *Anal. Biochem. 150*, 258−263.
24. Eftink, M. R. (1994) *Biophys. J. 66*, 482−501.
25. Pace, C. N., and Scholtz, J. M. (1997) in *Protein Structure: A Practical Approach* (Creighton, T. E., Ed.) Chapter 12, Oxford University Press, New York.
26. Novokhatny, V., Medved, L., Mazar, A., Marcotte, P., Henkin, J., and Ingham, K. (1992) *J. Biol. Chem. 267*, 3878−3885.
27. Becktel, W. J., and Schellman, J. A. (1987) *Biopolymers 26*, 1859−1877.
28. Chen, R. (1965) *Science 150*, 1593−1595.
29. Ware, W. R., Doemeny, L. J., and Nemzek, T. L. (1973) *J. Phys. Chem. 77*, 2038−2048.
30. Hui, M. H., and Ware, W. R. (1976) *J. Am. Chem. Soc. 98*, 4712−4717.
31. O'Connor, D., and Phillips, D. (1984) in *Time Correlated Single Photon Counting*, Academic Press, San Diego, CA.

32. Holzwarth, A. R. (1995) *Methods Enzymol. 246*, 334−362.
33. Abagyan, R. A., and Totrov, M. M. (1994) *J. Mol. Biol. 235*, 983−1002.
34. Abagyan, R. A., Totrov, M. M., and Kuznetsov, D. N. (1994) *J. Comput. Chem. 15*, 488−506.
35. Nicholson, H., Anderson, D. E., Dao-pin, S., and Matthews, B. W. (1991) *Biochemistry 30*, 9816−9828.
36. Cornette, J. L., Cease, K. B., Margalit, H., Spouge, J. L., Berzofsky, J. A., and DeLisi, C. (1987) *J. Mol. Biol. 195*, 659−685.
37. Donnelly, D., Overington, J. P., and Blundell, T. L. (1994) *Protein Eng. 7*, 645−653.
38. Weaver, L. H., and Matthews, B. W. (1987) *J. Mol. Biol. 193*, 189−199.
39. Kosower, E. M., Giniger, R., Radkowsky, A., Hebel, D., and Shusterman, A. (1986) *J. Phys. Chem. 90*, 5552−5557.
40. Mchaourab, H. S., Lietzow, M. A., Hideg, K., and Hubbel, W. L. (1996) *Biochemistry 35*, 7692−7704.
41. Matthews, B. W. (1995) *Adv. Protein Chem. 46*, 249−278.
42. McLaughlin, M. L., and Barkley, M. D. (1997) *Methods Enzymol. 278*, 190−202.
43. Chen, Y., Liu, B., Yu, H.-T., and Barkley, M. D. (1996) *J. Am. Chem. Soc. 118*, 9271−9278.

BI991331V